First publ. in: Physica / A [Statistical Mechanics], Vol. 201 (1993), pp. 207-222

Light scattering spectroscopy of the liquid–glass transition: comparison with idealized and extended mode coupling theory

H.Z. Cummins[a], W.M. Du[a], M. Fuchs[b], W. Götze[b], A. Latz[b,1], G. Li[a] and N.J. Tao[a,2]

[a]*Physics Department, City College of New York - CUNY, New York, NY 10031, USA*
[b]*Physics Department, Technische Universität München W-9646 Garching, Germany*

Light scattering experiments were performed on several fragile glass-forming materials at temperatures ranging from above the melting temperature T_m to below the calorimetric glass transition temperature T_g in the frequency range 0.2 GHz to 4000 GHz. The experimental susceptibility spectra $\chi''(\omega)$ exhibit both the form and the scaling properties predicted by the idealized mode coupling theory. In particular, the scaling frequency ω_σ was found to obey the power law $\omega_\sigma \propto |T - T_C|^{2a}$ for three different materials, confirming the predicted "critical slowing down" as $T \to T_C$ from either above or below. At low frequencies and temperatures the spectra deviate from the predictions due to the neglect of ergodicity-restoring activated transport (hopping) processes. We have therefore reanalyzed the data using the extended version of the theory, including activated transport.

1. Introduction

The dynamics of supercooled liquids approaching the liquid–glass transition has been the subject of intensive study in recent years, stimulated by the development of the mode coupling theory (MCT) which provides a series of predictions for the correlation functions and susceptibility spectra of the density fluctuations (for extensive reviews of MCT, see [1]). Several crucial experimental tests of MCT have been performed using inelastic neutron scattering techniques as described, for example, in the 1988 workshop "Dynamics of Disordered Materials I" [2].

In a light scattering study of the ionic glass former calcium potassium nitrate (CKN), we found that beyond the strong Brillouin components the spectrum

[1] Present address: Institute for Physical Science, University of Maryland, College Park, MD 20742, USA.

[2] Present address: Department of Physics, Florida International University, Miami, FL 33199, USA.

contains a weak wing with a self-similar form characteristic of power-law spectra [3]. This wing is not part of the usual Brillouin spectrum; it is part of a broad continuum culminating in a feature at ~1000 GHz which, at low temperatures, is sometimes designated as the "Boson peak".

By extending these spectra to span a frequency range exceeding four decades, we have been able to reveal the evolution of the structural relaxation dynamics with cooling. In particular, we have been able to test the MCT scaling predictions, and to demonstrate the critical slowing down of β-relaxation predicted by the theory.

2. Experiments

The light-scattering experiments are performed in depolarized near-backscattering geometry ($\theta \cong 173°$) where first-order scattering from LA and TA modes (the usual Brillouion scattering) is forbidden. The materials are either vacuum distilled or filtered into cylindrical glass sample cells and flame sealed. A 488 nm single-mode argon-ion laser provides the incident light. At each temperature the scattered light is analyzed with a six-pass Sandercock tandem Fabry–Perot interferometer at four different mirror separations (typically, $d = 0.5$, 3.5, 10 and 25 mm), and also with a conventional tandem Raman grating spectrometer (Spex 1401). The five sets of depolarized backscattering spectra are then combined to produce composite wideband optical spectra covering a frequency range of over four decades, from ~0.2 GHz to ~4000 GHz. Fig. 1 shows a log–log plot of such composite spectra for CKN [4]. Note that at low temperatures there is a weak LA peak near 20 GHz due to slight leakage of this very strong signal through the polarizer.

The composite $I(\omega)$ spectra are converted to susceptibility spectra $\chi''(\omega)$ by dividing out the Bose factor. The result for CKN is shown in fig. 2 [4,5]. Similar results were obtained for salol [6] and propylene carbonate [7], which, like CKN, are fragile glass-formers [8]. These $\chi''(\omega)$ spectra exhibit three obvious characteristics: (1) there is a strong high-frequency peak (near 3000 GHz for CKN) which is only weakly temperature-dependent, (2) there is a second peak which is close to the high-frequency peak at high temperature, moves rapidly toward lower frequency with decreasing temperature, and for CKN disappears from our spectral window at ~120°C, (3) there is a minimum in $\chi''(\omega)$ between these two peaks at some frequency ω_{min} where $\chi''(\omega_{min}) = \chi''_{min}$. It becomes weaker and also moves to lower frequencies with decreasing temperature. At temperatures below ~100°C, the CKN $\chi''(\omega)$ spectra exhibit a "knee" (i.e. a downward concave shape) rather than a minimum. The position and χ'' value of the knee will be designated as ω_e and χ''_e.

The intensity of $\chi''(\omega)$ at the minimum (χ''_{min}) and at the knee (χ''_e) are

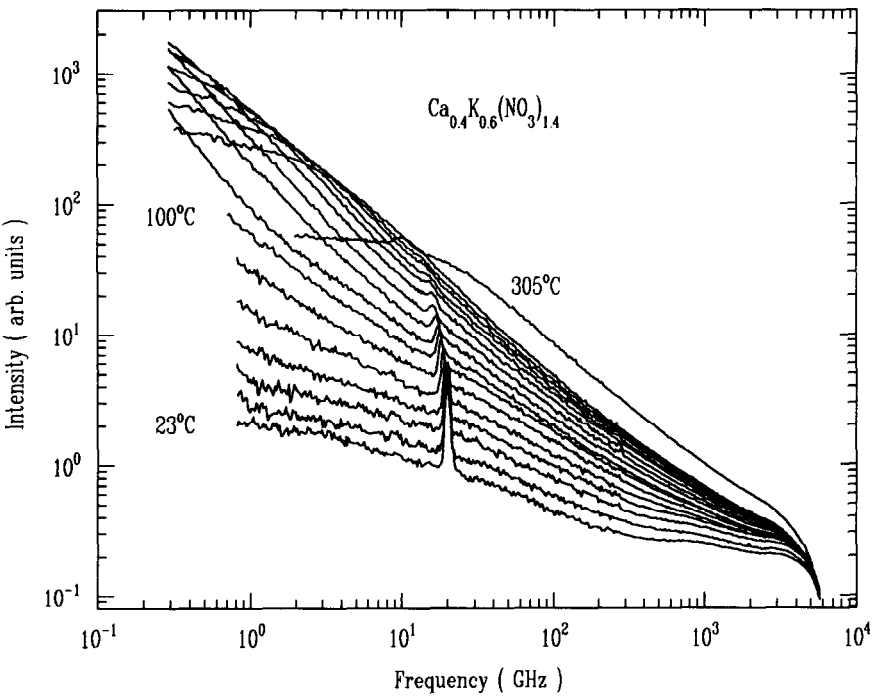

Fig. 1. Composite depolarized $\theta = 173°$ interferometric and Raman-scattering spectra of CKN. The temperatures are (top to bottom) 305, 195, 180, 170, 160, 150, 140, 130, 120, 110, 100, 90, 80, 70, 60, 45, and 23°C. The small peaks appearing at ~20 GHz are due to slight leakage of the intense LA Brillouin components. (From ref. [4].)

strongly enhanced relative to a white noise background spectrum which can be estimated by linear extrapolation of the low-frequency wing of the microscopic peak in the susceptibility spectrum to low frequencies. Note that it is this large enhancement of $\chi''(\omega)$ near the minimum above the white noise level, rather than the fact that the minimum exists, that demonstrates the significance of the β-relaxation process.

These features are consistent with MCT predictions to be discussed below which identify the high-frequency peak as the microscopic peak at Ω_0, the low-frequency peak as the primary α-relaxation peak, and the region surrounding the $\chi''(\omega)$ minimum at high temperature (or the knee at lower temperatures) as the intermediate β-relaxation.

In the depolarized backscattering geometry where first-order light scattering from LA and TA modes is forbidden, two other light-scattering mechanisms are allowed: first-order scattering from orientational fluctuation of anisotropic molecules, and second-order interaction-induced scattering.

MCT predicts that within the β-relaxation region these contributions to the

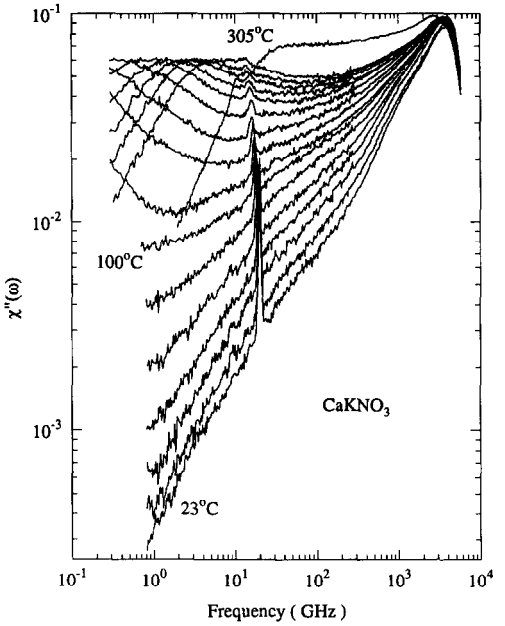

Fig. 2. Composite susceptibility spectra $\chi''(\omega)$ for CKN derived from the composite spectra of fig. 1. (From ref. [5].)

light-scattering intensity can be written as $I(\omega) = I_0(\omega) + h_{1s}G''(\omega)$. Here $G''(\omega)$ is the β-relaxation spectrum to be discussed below, h_{1s} is an amplitude which depends smoothly on temperature, and $I_0(\omega)$ is a slowly varying background spectrum. In the following sections we shall restrict our analysis to the β-relaxation region and neglect I_0, so that we will express $I(\omega)$ as

$$I(\omega) = h_{1s}G''(\omega)\,. \tag{2.1}$$

3. Mode coupling theory

3.1. Idealized MCT

The mode coupling theory, first proposed in 1984 [9,10] as a possible explanation of the liquid–glass transition, is based on a set of Mori–Zwanzig (or generalized oscillator equations of motion for $\phi_q(t)$, the normalized autocorrelation functions of the density fluctuations modes $\rho_q(t)$,

$$\ddot{\phi}_q(t) + \Omega_q^2\phi_q(t) + \Omega_q^2 \int_0^t M_q(t-t')\,\dot{\phi}_q(t')\,\mathrm{d}t' = 0\,. \tag{3.1}$$

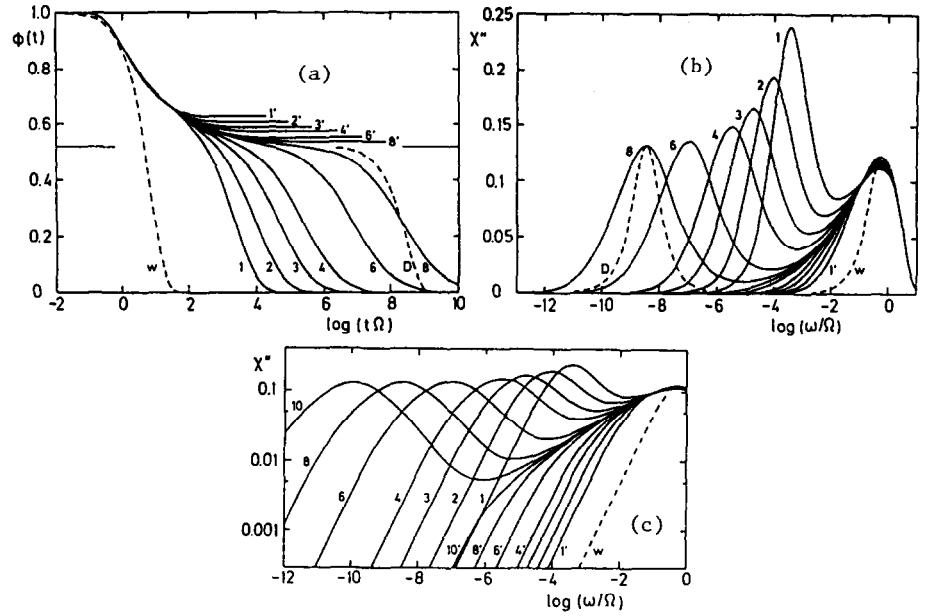

Fig. 4. Correlation functions $\phi(t)$ (a) and susceptibility spectra $\chi''(\omega)$ (linear scale (b) and log scale (c)) for the F_{13} model with $\gamma = 5\Omega_0$. Curves labeled $1, 2, 3, \ldots$, (liquid) or $1', 2', 3', \ldots$, (glass) lie on a straight-line trajectory in the $(V^{(1)}, V^{(3)})$ parameter space, as indicated in fig. 3. The parameter values corresponding to (n/n') are: $V^{(1)} = V_1^c \mp 0.730/2^n$ and $V^{(3)} = V_3^c \pm 1.424/2^n$. The critical point is at $V_1^c = 0.9549$, $V_3^c = 4.1733$ where $\lambda = 0.72$ and $f_c = 0.52$, which is indicated by a horizontal line in (a). A Debye curve $\phi(t) = \exp(-t/\tau)$ matching the short-time dynamics is indicated in (a) by the dashed line (w). In (a) and (b), Debye α-relaxation results corresponding to curve 8 are indicated by dashed lines labelled (D) to illustrate the stretching in the F_{13} model. In (b) and (c), a dashed line (w) has been added which is an estimate of the white noise level, matched to the high-frequency microscopic band at $\omega \sim \Omega_0$.

$$\sigma + \lambda G^2(t) = \frac{\mathrm{d}}{\mathrm{d}t} \int_0^t G(t - t')\, G(t')\, \mathrm{d}t' \,, \tag{3.6}$$

where the separation parameter $\sigma \propto (T_C - T)$ measures the distance from T_C. The exponent parameter λ ($\frac{1}{2} \leqslant \lambda \leqslant 1$) in eq. (3.6) is a well-defined but complicated function of the vertices. In data analysis with the idealized MCT, λ appears as the only fit parameter. Once λ is specified, eqs. (3.5) and (3.6) determine the full structure of $\phi_q(t)$ in the intermediate time regime $1/\Omega_q \ll t \ll \tau_\alpha$, apart from the numerical factors f_q^c and h_q. The exponent parameter λ, in turn, fixes the two exponents of MCT: the critical exponent $a (0 < a < 0.395)$ and the von Schweidler exponent $b (0 < b < 1)$. For T above but near T_C, the

Ω_q is a microscopic (phonon) frequency and $M_q(t-t')$ is the correlation function of the random forces. In the original (idealized) version of the theory, $M_q(t-t')$ is split into a "fast" regular damping term $\gamma_q\delta(t-t')$ and a memory function $m_q(t-t')$ which represents structural relaxation processes. Eq. (3.1) then becomes

$$\ddot{\phi}_q(t) + \Omega_q^2\phi_q(t) + \Omega_q^2\gamma_q\dot{\phi}_q(t) + \Omega_q^2\int_0^t m_q(t-t')\,\dot{\phi}_q(t')\,\mathrm{d}t' = 0\,. \tag{3.2}$$

In these equations (3.2) (one for each q), the memory function $m_q(t-t')$ appears as a quantity proportional to a retarded damping force.

This set of integro-differential equations can be closed by invoking Kawasaki's factorization approximation and expressing $m_q(t)$ in terms of products of density correlation functions,

$$m_q(t) = \sum_{q_1} V^{(1)}(q, q_1)\,\phi_{q_1}(t) + \sum_{q_1,q_2} V^{(2)}(q, q_1, q_2)\,\phi_{q_1}(t)\,\phi_{q_2}(t) + \cdots, \tag{3.3}$$

which is the mode coupling approximation.

The vertices or coupling coefficients $V^{(i)}$ in eq. (3.3) are expressed in terms of the structure factors $S(q)$. The structure factors, and therefore all the vertices, are assumed to be smooth functions of the physical control parameters such as temperature. The nonlinear coupled set of eqs. (3.2) and (3.3) are then to be solved self-consistently.

Simplified schematic models can be constructed by considering a single mode, producing a single schematic equation of motion,

$$\ddot{\phi}(t) + \Omega_0^2\phi(t) + \Omega_0^2\gamma\dot{\phi}(t) + \Omega_0^2\int_0^t [V^{(1)}\phi(t-t') + V^{(2)}\phi^2(t-t') + \cdots]\dot{\phi}(t)\,\mathrm{d}t' = 0\,. \tag{3.4}$$

The simplest such schematic model, the F_2 model, retains only the quadratic term $V^{(2)}\phi^2(t)$ in eq. (3.4). As shown in the original 1984 MCT papers [9,10], the F_2 schematic model contains a singularity (the glass-transition singularity or GTS) at $V^{(2)} = 4$. As $V^{(2)}$ increases with decreasing temperature, the singularity occurs at a "crossover temperature" T_C. For $T \leq T_C$, the $t\to\infty$ limit of $\phi(t)$ no longer decays to zero, but instead approaches a limit called the nonergodicity parameter $f(T)$.

For $T > T_C$, this F_2 model predicts exponential long-time decay, i.e. there is no stretching of the final α-relaxation. The next simplest model, the F_{12} model

for which $m(t) = V^{(1)}\phi(t) + V^{(2)}\phi^2(t)$ does produce stretching and has therefore been used frequently in subsequent studies of schematic models.

We have solved the schematic MCT eq. (3.4) for the F_{13} model [11] where $m(t) = V^{(1)}\phi(t) + V^{(3)}\phi^3(t)$. Fig. 3 shows part of the phase diagram in the $(V^{(1)}, V^{(3)})$ parameter space where the liquid–glass boundary is indicated by the solid line. Solutions to eq. (3.4) for the $(V^{(1)}, V^{(3)})$ values indicated by the trajectory of points in fig. 3 are shown in fig. 4a. Note that for the $(V^{(1)}, V^{(3)})$ values in the liquid $(1, 2, \ldots, 8)$, $\phi(t)$ eventually decays to zero, while for the glass values $(8', 7', \ldots, 1')$, $\phi(t)$ arrests at a non-zero value $f(T)$. (At $T = T_C$, $f = f_c = 0.52$.)

Fourier transformation of these $\phi(t)$ curves which gives $S_q(\omega)$, followed by multiplication by ω, produces the $\chi''(\omega)$ susceptibility spectra shown in fig. 4b (linear scale) and 4c (log scale). Note the similarity of the log–log plot of $\chi''(\omega)$ in fig. 4c to the experimental CKN data in fig. 2.

Analysis of the full MCT equations (3.2) and (3.3) has shown that in the intermediate β-relaxation region around the susceptibility minimum, the form of $\phi_q(t)$ is independent of the detailed structure of the $V^{(i)}$, and exhibits the factorization property

$$\phi_q(t) = f_q^c + h_q G(t) . \tag{3.5}$$

The β-correlator $G(t)$ obeys the equation of motion

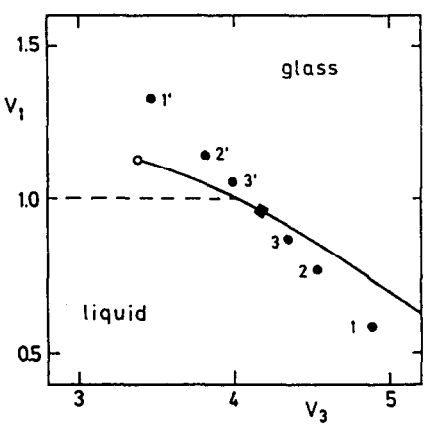

Fig. 3. Part of the phase diagram for the F_{13} schematic model of eq. (3.4) with $m(t) = V^{(1)}\phi(t) + V^{(3)}\phi^3(t)$. The solid line terminating in a circle is a type B transition line (where the nonergodicity parameter changes abruptly) on which $\lambda \geq \frac{1}{2}$, $a \leq 0.395$. The dashed line is a type A transition line (where the nonergodicity parameter changes continuously) which is not relevant for this discussion.

form of $\phi_q(t)$ in the intermediate time regime exhibits power-law decay towards a plateau: $\phi_q(t) \approx f_q^c + h_q(t/t_0)^{-a}$, followed by a second power-law decay: $\phi_q(t) \approx f_q^c - s_q(t/t_0)^b$ (the von Schweidler decay), which is the early part of the α-relaxation. Similarly, the spectrum $S(q, \omega)$ is predicted to exhibit two power-law regions.

This analysis predicts that for $T > T_C$ the susceptibility minimum should fall between two power-law regions: $\chi''(\omega) \propto \omega^a (\omega > \omega_{min})$ and $\chi''(\omega) \propto \omega^{-b} (\omega < \omega_{min})$ while for $T < T_C$ the knee locates a crossover from $\chi''(\omega) \propto \omega^a$ to $\chi''(\omega) \propto \omega$. Note that the $\chi''(\omega) \propto \omega$ region for $T < T_C$ reflects the arrest of α relaxation. Referring to fig. 4a, for $T < T_C$, $\phi(t)$ decays to a plateau and arrests, so that $S(q, \omega) = \int_{t=0}^{\infty} \cos(\omega, t)\ \phi(t)\, dt$ must be independent of ω for small (nonzero) ω. Therefore $\chi''(\omega) = \omega S(q, \omega) \propto \omega$.

From eqs. (3.5) and (3.6) one also finds that the susceptibility spectra factorize, and obey a scaling law,

$$\chi''(\omega) = h_q |\sigma|^{1/2} \hat{\chi}''_{\pm}(\omega/\omega_\sigma) , \tag{3.7}$$

where $\omega_\sigma \propto |\sigma|^{1/2a}$.

The two susceptibility master functions $\hat{\chi}''_+$ for the glass ($T < T_C$) and $\hat{\chi}''_-$ for the liquid ($T > T_C$) can be calculated numerically once λ is specified [12]. Eq. (3.7) then predicts that for either $T > T_C$ or $T < T_C$, all susceptibility spectra should scale onto a single master curve, with the scaling frequency $\omega_\sigma \to 0$ as $T \to T_C$ from either above or below. Furthermore, eq. (3.7) predicts that χ''_{min} and ω_σ (or ω_{min}) obtained from the scaling procedure for $T > T_C$, and χ''_e and ω_e for $T < T_C$ should obey

$$\chi''_{min} \propto \chi''_e \propto |\sigma|^{1/2} = C_\sigma , \qquad \omega_{min} \propto \omega_e \propto |\sigma|^{1/2a}/t_0 = \omega_\sigma . \tag{3.8}$$

3.2. Extended MCT

The extended version of MCT [13] includes a current term δ in the kernel $M(t - t')$ in eq. (3.1) which represents ergodicity-restoring activated hopping processes ignored in the simpler idealized version of the theory.

In the idealized MCT, the Fourier transform of $M_q(t)$ in eq. (3.1) is $M_q(\omega) = [i\gamma_q + m_q(\omega)]$, where $m_q(\omega)$ is the Fourier transform of $m_q(t)$ in eq. (3.3), which represents cage effects. In the extended MCT, one has

$$M_q(\omega) = [i\gamma_q + m_q(\omega)]/\{1 - \delta_q(\omega)\, \Omega_q^2 [i\gamma_q + m_q(\omega)]\} , \tag{3.9}$$

where $\delta_q(\omega)$ is the Fourier transform of

$$\delta_q(t) = \sum_{q_1,q_2} V'(q, q_1, q_2)\, \dot{\phi}_{q_1}(t)\, \dot{\phi}_{q_2}(t) + \cdots, \tag{3.10}$$

which represents, to leading order, the coupling of density fluctuations to activated transport processes through the temperature-dependent hopping kernel δ_q. The terms not written explicitly in eq. (3.10) contain mode couplings to longitudinal and transverse current correlators. For the latter, equations of motion have been derived which are similar to the one for density [13].

As T decreases towards T_C, the system will follow a trajectory in the (σ, δ) space as illustrated schematically in fig. 5 by trajectories such as C_1 or C_2 where the hopping rate δ has been assumed to follow an Arrhenius law. In the extended theory the abrupt transition at $\sigma = 0$ is replaced by a continuous crossover from liquid dynamics for $\sigma < 0$ to glassy dynamics for $\sigma > 0$ within a transition region centered at the glass singularity at (0, 0). Although the GTS is not directly traversed, it nonetheless controls the dynamics in the vicinity of the crossover.

In fig. 6 we show solutions to the schematic F_{13} model of fig. 4, but now including the δ term. Note that here, in contrast to fig. 4, $\phi(t)$ always decays to zero at sufficiently long times. The complete structural arrest at $\sigma \geq 0$ predicted by the idealized theory is cut off by the inclusion of current terms as first noticed by Das and Mazenko [14]. As seen in figs. 6b and 6c, the α peak and $\chi''(\omega)$ minimum no longer disappear at T_C. Instead, the α peak moves continuously to lower frequency with decreasing temperature as observed, for example, in dielectric susceptibility experiments [15].

In the extended MCT, $\phi(t)$ in the β-relaxation region still obeys the factorization property of eq. (3.5). However, the equation of motion for $G(t)$ is now given by

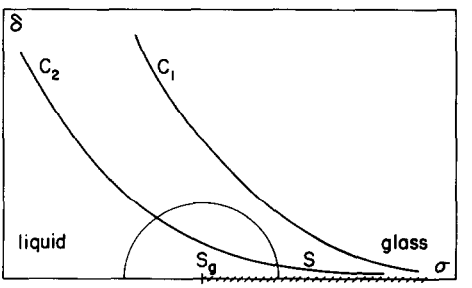

Fig. 5. Sketch of the $(\sigma, \delta t_0)$ parameter space for the MCT equations. S_g locates the glass transition singularity at (0, 0) and the shaded line S is the location of ideal glass states. C_1 and C_2 indicate possible paths followed by a system moving from left to right with decreasing temperature. (From ref. [13].)

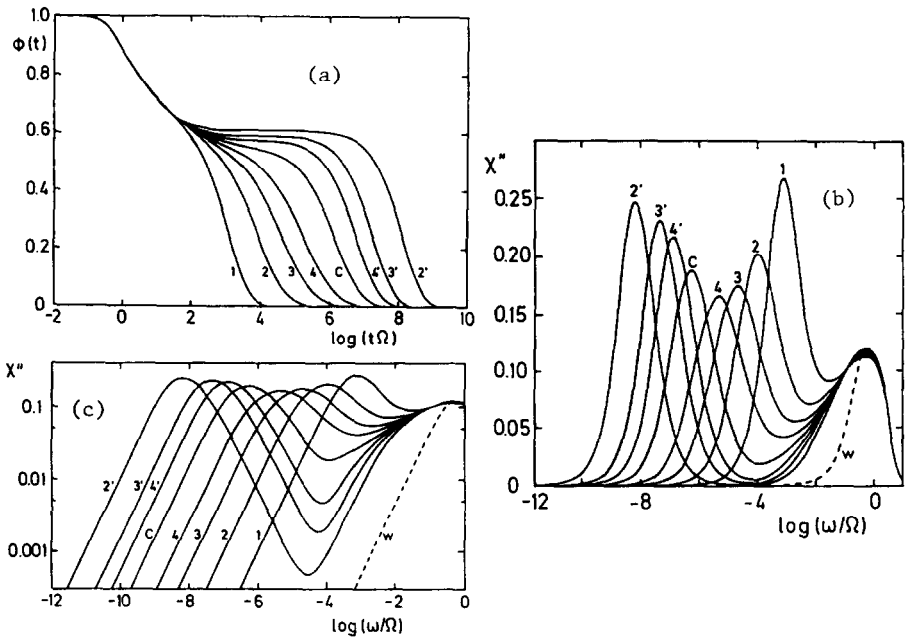

Fig. 6. $\phi(t)$ (a) and $\chi''(\omega)$ (linear scale (b) and log scale (c)) for the extended MCT version of the F_{13} model. The $(V^{(1)}, V^{(3)})$ values are the same as those in fig. 4. The hopping kernel was not calculated, but was approximated as $\delta(\omega) = i\delta$ with δ decreasing exponentially along the $(V^{(1)}, V^{(3)})$ trajectory from liquid to glass. The curves labelled c correspond to the critical values of $(V^{(1)}, V^{(3)})$ in fig. 4. Note that the α peak in $\chi''(\omega)$ moves continuously towards lower frequencies with decreasing T.

$$\sigma - \delta t + \lambda G^2(t) = \frac{\mathrm{d}}{\mathrm{d}t} \int_0^t G(t - t')\, G(t')\, \mathrm{d}t' \,, \tag{3.11}$$

instead of by eq. (3.6). In eq. (3.11), σ is the previously introduced separation parameter which quantifies the cage effect. δ, designated as the hopping parameter, is a smoothly varying quantity determined by the kernels $\delta_q(t)$. Notice that in the β regime the dependence of the solution on the many vertices is reduced to the dependence on the two numbers σ and δ. These quantities play the role of the relevant control parameters, governing the physics near the GTS for intermediate times or frequencies. The properties of eq. (3.11) and its solutions have been discussed in detail by Fuchs et al. [16].

Once λ has been specified, the β-correlator $G(t)$ determined by eq. (3.11) (and the susceptibility function $\chi''(\omega)$) are fixed by two parameters: the separation parameter σ and the hopping rate δ. These parameters can be

determined by fits to experimental data, as described briefly in the following section.

4. Data analysis

4.1. α-relaxation

The low-frequency peaks visible in the CKN $\chi''(\omega)$ spectra of fig. 2 for $T \geqslant 120°C$ were fit to $\chi''(\omega)$ derived from stretched exponentials $\phi(t) = f\,e^{-(t/\tau)^{\beta}}$. The results showed that α-scaling is obeyed, with the Kohlrausch stretching exponents $\beta \approx 0.55$ (CKN), $\beta \approx 0.84$ (salol), and $\beta \approx 0.77$ (PC). Combining our salol data with the dielectric data of Dixon et al. [15] indicates that for salol, β increases from ~0.55 near T_g to ~0.84 at ~256 K and then remains constant. We found no tendency for β to increase towards $\beta = 1$ at high temperatures for any of the three materials studied. The relaxation times deduced from our light scattering data, the dielectric data, and the temperature dependence of the viscosity were also in good agreement.

4.2. β-relaxation

Susceptibility spectra in the region of the minimum were first fit to the approximate interpolation formula

$$\chi''(\omega) = \chi''_{\min}[b(\omega/\omega_{\min})^a + (\omega_{\min}/\omega)^b]/(a+b) \tag{4.1}$$

to provide estimates of the critical exponents a and b and of the exponent parameter λ, as well as of $\omega_{\min}$ and $\chi''_{\min}$. Subsequently, the master curves $\hat{\chi}''_{\pm}(\omega/\omega_\sigma)$ were constructed following the numerical procedure in ref. [12], and the data was rescaled onto the master curves as shown for salol in fig. 7. This scaling procedure then gave the scaling frequency ω_e and scaling amplitude χ''_e for each temperature.

The MCT predictions of eq. (3.8) imply that plots of $(\omega_{\min})^{2a}$ and $(\omega_e)^{2a}$ vs. T should give straight lines that extrapolate to 0 at $T = T_C(\sigma = 0)$: $\omega_{\min}^{2a} \propto \omega_e^{2a} \propto \omega_\sigma^{2a} \propto |\sigma| \propto |T - T_C|$. Similarly, the prediction for χ'' is $\chi''^2_{\min} \propto \chi''^2_e \propto C_\sigma^2 \propto |\sigma| \propto |T - T_C|$. These plots for salol are shown in fig. 8 where the predicted linear temperature dependence and the extrapolation to zero at a common T_C is evident. The results of these fits for CKN, salol, and PC, are summarized in table I.

The idealized MCT fits to the unscaled $\chi''(\omega)$ spectra of CKN and salol in the β-relaxation region are shown in figs. 9a and 9c. Although the fits are generally good, systematic discrepancies occur for temperatures close to and below T_C

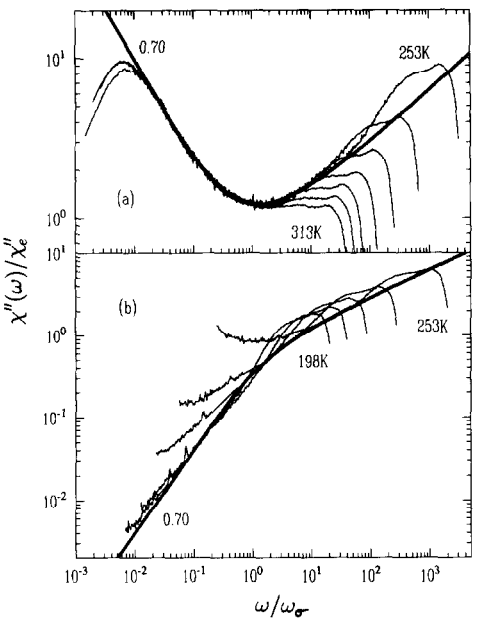

Fig. 7.

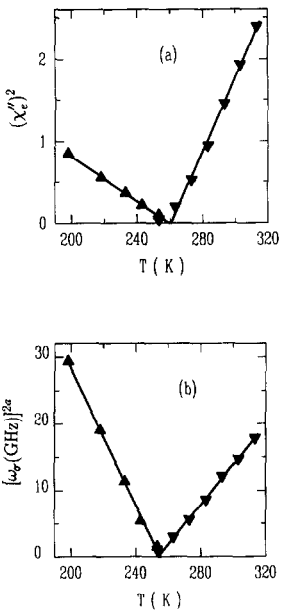

Fig. 8.

Fig. 7. Rescaled plots of the salol $\chi''(\omega)$ curves for (a) $T > T_C$ and (b) $T < T_C$. The thick curves are the $\lambda = 0.70$ master curves for $\sigma < 0$ and $\sigma > 0$. (From ref. [6].)

Fig. 8. Temperature dependence of $(\chi_e'')^2$ (a) and ω_σ^{2a} (b) both above and below T_C obtained from the scaling procedure shown in fig. 7. Extrapolation to zero locates T_C at 256 K. (From ref. [6].)

Table I
Idealized MCT analysis results.

Material	T_g (K)	T_m (K)	T_C (K)	β ($T > T_C$)	a	b	λ
CKN	333	~438	378	0.55	0.27	0.46	0.81
salol	218	315	256	0.84	0.33	0.64	0.70
PC	160	218	187	0.77	0.29	0.51	0.78

near the lower end of our spectral window ($\nu \lesssim 10$ GHz). The tendency of the theoretical curves to fall systematically below the experimental data demonstrates the limitations of the idealized theory in which both the susceptibility minimum and the α peak disappear at T_C. As noted above, when hopping terms are included, the α peak and susceptibility minimum will still be present below T_C.

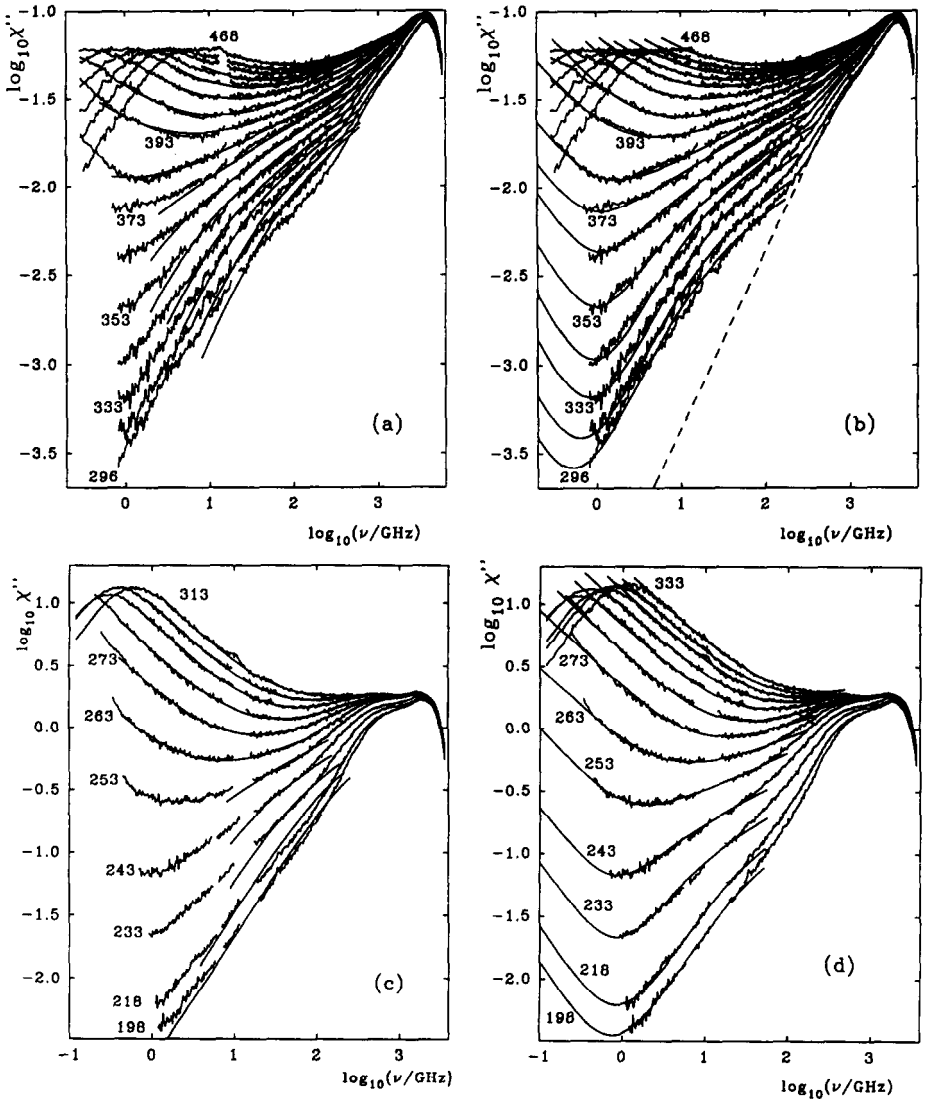

Fig. 9. Susceptibility spectra $\chi''(\omega)$ of CKN (a, b) and salol (c, d). The temperatures range from $T = 296$ K to 468 K for CKN and from $T = 198$ K to 313 K (c) or 333 K (d) for salol. The $\delta = 0$ idealized MCT fits for CKN with $\lambda = 0.81$ and for salol with $\lambda = 0.70$ are shown in (a) and (c), respectively. Note that at low frequencies and temperatures there are systematic errors indicating the limitations of the idealized theory. The full lines in (b) and (d) are fits with $\delta \neq 0$ β-relaxation functions of the extended MCT with $\lambda = 0.85$ (CKN) and $\lambda = 0.73$ (salol). The dashed line in (b) is an upper limit to the white-noise spectrum $\chi''(\omega) \propto \omega$ matched to the microscopic peak. (From ref. [17].)

4.3. *Extended MCT*

We have recently reanalyzed the CKN and salol $\chi''(\omega)$ data using the extended MCT approach [17]. At each temperature the parameters σ and δt_0 were adjusted to optimize the fit, using the idealized MCT fits for initial estimates of λ and $\sigma(T)$. The results, shown in figs. 9b and 9d, clearly provide much better fits to the data than the idealized MCT fits. (Details of the fitting procedure can be found in ref. [17].) Note that the extended MCT fits shown in fig. 9 predict the position of the susceptibility minimum for temperatures below T_C. Although the region of the predicted minimum is beyond the range of our tandem interferometer, it does fall within the spectral region accessible to a confocal interferometer and should be experimentally observable.

The extended MCT fits for CKN, shown in fig. 9b, determine the trajectory of CKN in the $(\sigma, \delta t_0)$ parameter space with decreasing temperature. In fig. 10 the $(\sigma, \delta t_0)$ values at each temperature are indicated by the circles, and the interpolated trajectory is indicated by the solid line.

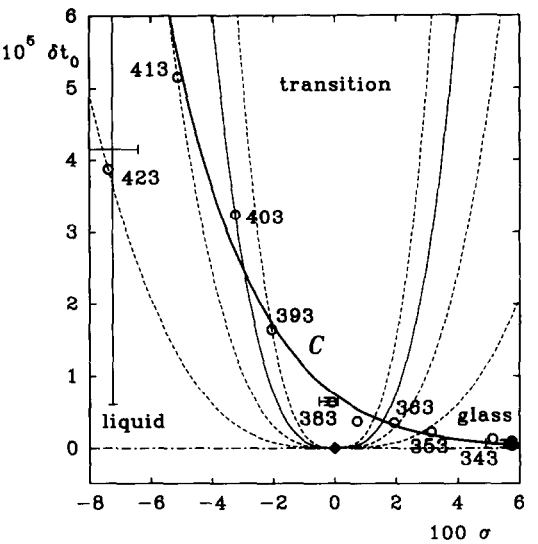

Fig. 10. $(\sigma, \delta t_0)$ parameter space explored by CKN in the temperature range 296 K$\leqslant T \leqslant$ 423 K. For 433 K $\leqslant T \leqslant$ 468 K, $\delta = 0$ could equally well be chosen. The data points are obtained from the fits of fig. 9b. Error bars in σ and S at $T = 333$, 383 and 423 K are estimated by visually comparing different fits. The bold solid line giving the approximate path C in the $(\sigma, \delta t_0)$ parameter space corresponds to an Arrhenius fit for $\delta(T)$ and a linear fit for $\sigma(T)$. The four generalized parabolas are scaling lines with $\sigma/\sigma_0 = \pm 2.15$, ± 1.36, ± 1 and ± 0.79 (listed by increasing steepness). They join in the glass transition singularity at $(\sigma, \delta) = (0, 0)$ marked by a diamond, which also separates the idealized liquid ($\sigma < 0, \delta = 0$) from the idealized glass ($\sigma > 0, \delta = 0$) scaling lines, both shown as chain curves. (From ref. [17].)

In carrying out the fits, we utilized the fact that in the extended MCT $\chi''(\omega)$ obeys a two-parameter scaling law [13],

$$\chi''(y\omega t_0, \sigma y^{2a}, \delta t_0 y^{1+2a}) = y^a \chi''(\omega, \sigma, \delta t_0) . \tag{4.2}$$

Eq. (4.2) establishes the scaling lines (i.e. trajectories in the $(\sigma, \delta t_0)$ plane where the $\log(\chi'')$ versus $\log(\omega)$ plots have the same shape) as a set of generalized parabolas $\delta t_0 = c|\sigma|^{(1+2a)/2a}$ passing through the GTS at (0, 0). The dimensionless hopping rate δt_0 also introduces a natural scale for σ: $\sigma_0 = (\delta t_0)^{2a/(1+2a)}$. Several scaling lines are indicated in fig. 10 for different values of σ/σ_0. The scaling line for $\sigma/\sigma_0 = 1$ delineates the crossover region separating regions of liquid dynamics and glassy dynamics. For CKN, this crossover region extends from ~363 K to 393 K. For salol it is much narrower.

5. Conclusions

Depolarized light scattering spectroscopy provides a highly effective probe of the dynamics of supercooled liquids approaching the liquid–glass transition. Susceptibility spectra of CKN, salol and PC are in good agreement with the predictions of the idealized MCT, demonstrating the critical slowing down of β relaxation as T_C is approached from either above or below. Systematic discrepancies found at low frequencies and temperatures were removed by utilizing the extended MCT which also eliminates the unphysical prediction of the idealized theory of complete α-relaxation arrest at T_C. In principle, application of the extended MCT in place of the idealized version used in previous analyses of experimental data should be followed whenever feasible, although a preliminary analysis with the simpler idealized theory can provide useful estimates.

Additional experiments are currently in progress in our laboratory, and other laboratories as well, to extend these studies to other fragile glassforming materials including polymers, and to less fragile materials such as glycerol and $ZnCl_2$. Such studies, in combination with neutron scattering, dielectric and photon correlation experiments, should eventually elucidate the range of validity of MCT and produce a deeper general understanding of the liquid–glass transition.

Acknowledgements

We wish to acknowledge helpful discussions with W. Petry, J. Wuttke, C.A. Angell, R. Pick and C. Dreyfus. Research at CCNY was supported by the U.S. National Science Foundation under grant No. DMR-9014344.

References

[1] (a) W. Götze and L. Sjögren, Rep. Prog. Phys. 55 (1992) 241;
(b) W. Götze, in: Liquids, Freezing and the Glass Transition, J.P. Hansen, D. Levesque and J. Zinn-Justin, eds. (North-Holland, Amsterdam, 1992) p. 287.
[2] Dynamics of Disordered Materials, Springer Proceedings in Physics, vol. 37, D. Richter, A.J. Dianoux, W. Petry and J. Texeira, eds. (Springer, Berlin, 1989).
[3] N.J. Tao, G. Li and H.Z. Cummins, Phys. Rev. Lett. 66 (1991) 1334.
[4] G. Li, W.M. Du, X.K. Chen, H.Z. Cummins and N.J. Tao, Phys. Rev. A 45 (1992) 3867.
[5] G. Li, W.M. Du, J. Hernandez and H.Z. Cummins, Phys. Rev. E (1993), submitted.
[6] G. Li, W.M. Du, A. Sakai and H.Z. Cummins, Phys. Rev. A 46 (1992) 3343.
[7] W.M. Du, G. Li, H.Z. Cummins, J. Toulouse and L. Knauss, unpublished.
[8] C.A. Angell, J. Non-Cryst. Solids 131–133 (1991) 13.
[9] E. Leutheusser, Phys. Rev. A 29 (1984) 2765.
[10] U. Bengtzelius, W. Götze and A. Sjölander, J. Phys. C 17 (1984) 5915.
[11] W. Götze and L. Sjögren, J. Phys. C 17 (1984) 5759;
W. Götze and R. Haussmann, Z. Phys. B 72 (1988) 403.
[12] W. Götze, J. Phys. Cond. Matt. 2 (1990) 8485.
[13] W. Götze and L. Sjögren, Z. Phys. B 65 (1987) 415; J. Phys. C 21 (1988) 3407.
[14] S.P. Das and G.F. Mazenko, Phys. Rev. A 34 (1986) 2265.
[15] P.K. Dixon, L. Wu, S.R. Nagel, B.D. Williams and J.P. Carini, Phys. Rev. Lett. 65 (1990) 1108;
P.K. Dixon, Phys. Rev. B 42 (1990) 8179.
[16] M. Fuchs, W. Götze, S. Hildebrand and A. Latz, J. Phys. Cond. Matt. 4 (1992) 7709.
[17] H.Z. Cummins, W.M. Du, M. Fuchs, W. Götze, S. Hildebrand, A. Latz, G. Li and N.J. Tao, Phys. Rev. E 47 (1993) 1727.